Title

A combined multi-reference pump-probe simulation method with application to XUV signatures of ultrafast methyl iodide photodissociation

Journal

The Journal of Chemical Physics, 151(12)

ISSN

0021-9606

Authors

Wang, Han

Odelius, Michael

Prendergast, David

Publication Date

2019-09-28

DOI

10.1063/1.5116816

Peer reviewed

A combined multi-reference pump-probe simulation method with application to XUV signatures of ultrafast methyl iodide photodissociation

Han Wang,[1] Michael Odelius,[2] and David Prendergast[1,3,a)]

AFFILIATIONS

[1]Chemical Sciences Division, Lawrence Berkeley National Laboratory, Berkeley, California 94720, USA
[2]Department of Physics, Stockholm University, AlbaNova University Center, SE-106 91 Stockholm, Sweden
[3]The Molecular Foundry, Lawrence Berkeley National Laboratory, Berkeley, California 94720, USA

Note: This paper is part of the JCP Special Collection on Ultrafast Spectroscopy and Diffraction from XUV to X-ray.
[a)]**Email:** dgprendergast@lbl.gov

ABSTRACT

UV pump-XUV/X-ray probe measurements have been successfully applied in the study of photo-induced chemical reactions. Although rich element-specific electronic structure information is accessible within XUV/X-ray (inner-shell) absorption spectra, it can be difficult to interpret the chemistry directly from the spectrum without supporting theoretical simulations. A multireference method to completely simulate UV pump-XUV/X-ray probe measurement has been developed and applied to study the methyl iodide photodissociation process. Multireference, fewest-switches surface hopping (FSSH) trajectories were used to explore the coupled electronic and ionic dynamics upon photoexcitation of methyl iodide. Interpretation of previous measurements is provided by associated multireference, restricted active space, inner-shell spectral simulations. This combination of multireference FSSH trajectories and XUV spectra provides an interpretation of transient features appearing in previous measurements within the first 100 fs after photoexcitation and validates the significant branching ratio in the final excited-state population. This methodology should prove useful for interpretation of the increasing number of inner-shell probe studies of molecular excited states or for directing new experiments toward interesting regions of the potential energy landscape.

INTRODUCTION

Inner-shell excited states, probed by XUV or X-ray Absorption Spectroscopy (XAS), reveal details of local electronic structure within molecules or materials, specific to a given element, which can be directly linked to useful atomic structural information, such as coordination number, bond length, angles between bonds, and oxidation states. As a probe within ultrafast pump-probe measurements, XAS is particularly attractive for revealing mechanistic details of photo-induced chemical reactions by following the time-evolution of various chemical groups through changes in their associated spectral features. There has been significant growth recently in application of table-top XUV/X-ray transient absorption spectroscopy[1–5] to probe valence and Rydberg core-excited states due to advances in high harmonic generation (HHG). A range of ultrafast photo-induced chemistry, such as bond breaking,[3,5] ring opening,[2,6] internal conversion (IC), and intersystem crossing (ISC),[4] has been studied with the aforementioned method. The bond breaking dynamics of CH_3I has been studied for a few decades with different experimental methods, such as photofragment spectroscopy,[7] magnetic circular dichroism spectroscopy,[8] mass spectrometer,[9] velocity map imaging spectroscopy,[10–13] and so forth. The C–I bond is expected to extend and break upon excitation of the valence electrons due to UV photon absorption. Previous work indicates excitation of the molecule into the $^3Q_0$ state when pumped with 266 nm UV light.[14] Subsequently, the electronic state is

proposed to undergo a transition into the $^1Q_1$ state as the system evolves toward a conical intersection, defined by a C–I bond length of ~2.4 Å,[15,16] where the transition rate is shown to be correlated with ν_6 degenerate methyl rocking modes.[8,17,18] The Mulliken[19] notations $^1Q_1$ and $^3Q_0$ are corresponding to 3E and $2A_1$ states[14,20] in the C_{3v} group symmetry, respectively. Transient XUV absorption spectroscopy measurements of CH_3I upon 266 nm UV excitation have been performed by Attar *et al.*[3] The real-time evolution of the XUV absorption spectra, with femtosecond resolution, during C–I bond breaking dynamics was probed near the iodine $N_{4,5}$-edge, from 45 to 60 eV (i.e., exciting I 4*d* inner-shell electrons into accessible excited states). The measured spectra confirm UV-induced photodissociation, releasing neutral iodine atoms in electronic ground, $I(^2P_{3/2})$, and excited, $I^*(^2P_{1/2})$, states, within ~90 fs of the UV excitation pump pulse.

Although rich electronic structure should be revealed within the transient XUV/X-ray absorption spectrum, it is difficult to interpret the chemistry directly from the measurement. Since the pump laser has a finite time duration, the transient XUV/X-ray absorption spectrum is necessarily convoluted with the pump. Furthermore, multiple transient spectral features appear in overlapping spectral ranges. In principle, since XAS measures the transition possibility of electrons from atomic core/inner-shell orbitals to unoccupied molecular orbitals, it is sensitive to details of the symmetry and character of the related molecular orbitals. On the one hand, this sensitivity means that transient XAS carries rich information on the molecular orbitals of the excited state, which could be utilized to understand the details of chemical dynamics after photoexcitation. On the other hand, without a detailed underlying model of the photoexcited dynamics, it is almost impossible to interpret the origin of different peaks simply from hypothetical changes in the molecular geometry.

Theoretical simulation of both the pump-induced ultrafast dynamics and the probed transient absorption spectrum is key to interpreting the rich information embedded within transient XUV/X-ray absorption spectra. With respect to the valence excited states induced by the pump, fewest switches surface hopping (FSSH) has been successfully applied to study the dynamics of photo-induced chemistry. The electronic excitation spectrum provided by linear-response time-dependent density functional theory (LR-TDDFT) has been used successfully in combination with FSSH to study ring-opening dynamics of 1,3-cyclohexadiene.[2] In the same work, the maximum overlap method (MOM)[21–23] together with restricted excitation window TDDFT (REW-TDDFT)[24] was also employed to calculate the XAS of the excited state during the bond breaking process. Since LR-TDDFT considers electronic excitations within a basis of single electron-hole pairs, the self-consistent field of the underlying valence-excited state was fixed using MOM, while efficient calculation of excitation energies relevant to core-excited states was provided again by LR-TDDFT, within a restricted energy window, by limiting the considered orbital space for holes to the corresponding inner-shell orbitals of the core-excited C atoms during this ring-opening process. However, it is well known that complete photodissociation often results in electronic excited states with clear multiconfigurational character. The accurate description of such a state can be obtained using spin-flip TDDFT[25] or a multireference method.

Multiconfiguration excited states can be accurately computed using complete active space self-consistent field (CASSCF) calculations with a judicious choice of orbitals to include in the active space[26] and the addition of corrections to include dynamic correlation from second-order perturbation theory (CASPT2).[27] Such calculations can obtain excited-state energies with only ~0.3 eV errors[28] for small- to medium-sized molecules. FSSH simulations based on the multireference method have been employed to accurately simulate electron and ion dynamics. The Surface Hopping including ARbitrary Couplings (SHARC) program[29–31] provides such a computational framework and has been applied in various systems.[32–35] However, we still lack the bridge between theoretical chemical dynamics simulations and pump-probe measurements based on XAS probes. In this work, we provide a methodology and a working example of simulated transient XUV/X-ray absorption spectroscopy (XAS) employing the current SHARC framework. We focus on the photo-induced bond breaking process of CH_3I as an illustrative example to explain the necessary workflow. In addition, the high atomic number of the I atom and the XUV probe of its 4*d* inner-shell electrons require accounting for strong spin-orbit (SO) interactions, both for the valence and core orbitals, respectively. In combination, the multiconfigurational and relativistic approach adopted here can reproduce the bond breaking process within FSSH trajectories, providing an electronic excitation spectrum with the correct spin-orbit splitting and associated transient XAS calculations that reproduce and interpret previous experimental measurements.

COMPUTATIONAL METHOD

Ground state XAS algorithm

The ground state XAS is calculated following the work of Josefsson *et al.*[36] and Delcey and Lundberg.[37] In the restricted active space self-consistent field (RASSCF) method, the multiconfigurational wavefunction is built up on the basis of electron configurations obtained by permutation of electrons occupying molecular orbitals in the active space, which is divided into subspaces, e.g., RAS1, RAS2, and RAS3. Core orbitals are placed in RAS1 active space allowing for at most one excitation. To keep the core orbitals that are initiated by orbitals from a Hartree-Fock (HF) calculation from rotating to valence orbitals, they can be frozen during the orbital optimization of multiconfigurational SCF calculations. Valence orbitals are placed in the RAS2 active space without constraint on their occupations. Possible higher energy orbitals are included in the RAS3 active space. After obtaining the RASSCF wavefunction, the dynamic electron correlation effects are included at the level of second order perturbation theory (RASPT2). The spin-orbit coupling effect and oscillator strength between the ground state and core excited state are calculated using the restricted active space state interaction (RASSI) approach.[38]

Multireference valence excited state XAS algorithm

Valence excited states can be created by the UV pump. The low-lying valence excited-state spectrum can be calculated using the CASPT2 method.[39] The XUV/X-ray probe is considered purely from the perspective of the new excitation channel that it exposes (see Fig. 1), the excitation of inner-shell or core orbitals into any unoccupied state. With respect to a pre-existing valence excited state, within

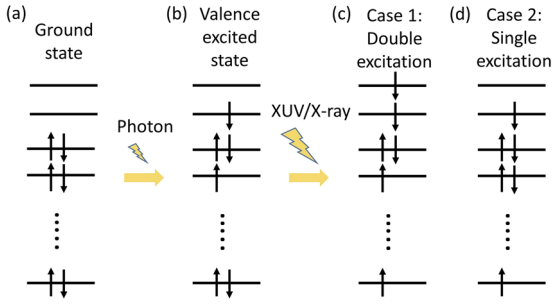

FIG. 1. A simplified diagram of the low-energy photon excitation and subsequent XUV/X-ray excitation process. The electronic structure of ground state (a), valence excited state induced by low-energy photon excitation (b), and the double excitation (c) and single excitation (d) state after XUV/X-ray excitation.

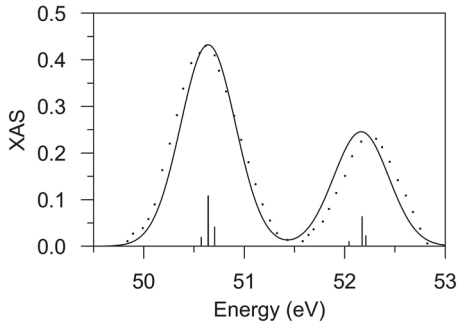

FIG. 2. XAS calculation of ground state CH_3I is shown in the solid line, where the dotted line is experimental data from Ref. 3. The peaks above 53 eV in the experimental spectrum[3] are Rydberg states, which are not well represented in the ANO-RCC-VTZP basis set. The experimental data are reproduced with permission from Attar *et al.*, J. Phys. Chem. Lett. **6**(24), 5072–5077 (2015). Copyright 2015 American Chemical Society. Further permissions related to the material excerpted should be directed to the ACS.

a simplified noninteracting electron model, we can imagine two possible final states for the core electron: (1) excitation into orbitals originally accessible in the ground state and (2) excitation into the vacated orbitals (holes) created by the UV excitation. In the first case, the molecule is placed in a doubly excited state, while, in the second case, the resulting final state is, ultimately, a singly excited state, due to annihilation of the valence hole. Of course, these core-excited states are more complicated due to the concomitant motion of the nuclei which in turn alters the electronic structure. For each moment in time, The CASPT2 method can handle both the single and double excitations, provided enough high-energy excited roots are calculated, although the relative accuracy may differ. With the pumped, valence excited state and final, valence and core excited states generated, we make use of the restricted active space state interaction (RASSI) module in OpenMolcas to calculate the oscillator strengths between these two sets of states. By numerically broadening the oscillator strength sticks with a Gaussian or Lorentzian function, a simulated absorption spectrum can be produced.

The state interaction calculation in OpenMolcas

Since the valence excited states and core+valence excited states are obtained from different calculations, the wavefunctions from both sets of calculations are not necessarily orthogonal. In fact, we must take particular care to avoid numerical errors here since the overlap between different wavefunctions is likely to be small, while the diagonal elements of the Hamiltonian may have very large values because, in this case, we consider the entire set of iodine core orbitals (e.g., E_{tot} = ~7000 hartree for CH_3I). We employ the original corrections to the overall Hamiltonian, defined in Ref. 38 for RASSI with spin-orbit (SO), as follows:

$$\Delta H_{IJ} = 0.5(\Delta E_I + \Delta E_J)S_{IJ},$$

where ΔE_I and ΔE_J are the energy shift for Ith and Jth RASSCF roots, S_{IJ} is the overlap matrix element, and ΔH_{IJ} is the energy shift for element H_{IJ}.

RESULT AND DISCUSSION

First, we study the XAS at the I $N_{4,5}$-edge for the electronic ground state of CH_3I, as shown in Fig. 2. Because of the strong spin-orbit coupling effect in CH_3I, the relativistic effects were included and treated in two steps, both based on the Douglas–Kroll Hamiltonian.[40,41] In the first step, scalar relativistic effects were included in the basis set generation[42,43] and used to determine "spin free" wavefunctions and energies of states with pure multiplicity through the use of the RASSCF method. Dynamic electron correlation effects were included in the RASPT2 method. Next, the optimized RASSCF/RASPT2 wavefunctions were used as the basis states in the restricted active space state interaction (RASSI)[38] module, where spin-orbit coupling was treated in the Atomic Mean Field (AMFI) approximation.[44] All the simulations in this work are carried out using the ANO-RCC basis set of VTZP quality.[42,43] As shown in Fig. 3, five iodine 4d orbitals in the RAS1 active space together with the 4 valence orbitals in the RAS2 space were used in the RASSCF/RASPT2 calculation. 4 orbitals in RAS2 space include two lone pair orbitals (I atom 5px and 5py orbitals) with slightly

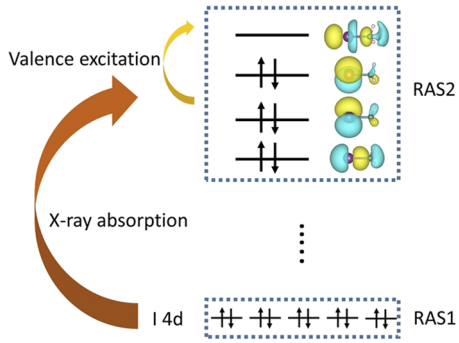

FIG. 3. Diagram of active space for XAS and FSSH calculation. In the FSSH calculation, 6 electrons and 4 RAS2 orbitals including two lone pair orbitals of I atom and C–I σ and σ^* orbitals are considered. The isosurface of the four valence orbitals are calculated with Hartree Fock theory. In the XAS calculation at each snapshot of the FSSH trajectory, 10 iodine 4d electrons are included in 5 RAS1 orbitals.

antibonding π^* character and both C–I σ and σ* orbitals. 10 singlet and 10 triplet roots are calculated by limiting the maximum occupation in the RAS1 active space (calculated using the OpenMolcas HEXS[45] tag), which calculates the excited states with one iodine 4d core hole. The oscillator strengths were calculated in the RASSI module. The vertical transition energies were obtained from state-averaged RASSCF and multistate RASPT2 calculations performed using all resulting singlet and triplet states. The core orbitals were constrained to their shape from the underlying HF calculation to ensure convergence. The core excitations were shifted in an *ad hoc* manner (−1.0 eV for RASPT2) to compensate for limitations in the wavefunctions. An overall 0.27 eV Gaussian convolution was applied to broaden the calculated spectrum and simulate the intrinsic experimental resolution.

Then, we performed nonadiabatic molecular dynamics simulation for the CH_3I molecule with Tully's fewest switches surface hopping theory[46] as implemented in the SHARC software package. Full multiple spawning[47] would be an alternative approach to simulate the bond breaking dynamics after UV excitation, but it is not our focus in this study and it might be considered in future work. The diagonal representation was used in the FSSH calculation, where the spin-mixed, fully adiabatic states are obtained by diagonalizing the electronic Hamiltonian matrix, which is built with 4 singlet and 4 triplet spin-free eigenstates and spin-orbit interaction. The velocity-Verlet algorithm with a time step of 0.1 fs was used in the integration of the nuclear motion. An energy-difference based correction[48] with parameter α = 0.1 hartree is used to take decoherence into consideration. The dynamics simulation was performed based on multistate, complete active-space second-order perturbation theory (MS-CASPT2) with an active space of 6 electrons in 4 orbitals calculated using OpenMolcas.[48] The isosurface of the four orbitals is shown in Fig. 3. Since the pump laser wavelength used in the experiment[3] is 266 nm, which is highly likely to excite CH_3I into the $^3Q_0$ state, we deliberately bias our excited state dynamics and only consider one electronic initial state for surface-hopping dynamics, which initially explores the $^3Q_0$ excited-state potential energy surface (PES). The initial velocities and geometries for the dynamics simulations were sampled from a Wigner distribution around the S0 minimum geometry with an effective temperature of 300 K.

Simulated transient XAS of FSSH trajectories

SHARC outputs the energy ordering index and energy of the active PES and the geometry of the molecule at each time point of the FSSH simulation. The on-the-fly XUV absorption spectrum is calculated with the geometry from every 0.5 fs snapshot of the trajectory. Note that the multiconfigurational wavefunction from the valence-excited FSSH calculation is not reused since core orbitals are absent from its active space, necessarily, for the sake of computational efficiency. Instead, the oscillator strength calculation has a similar setup as the ground state XAS calculation; however, as shown in Fig. 3, the active space used is larger: the transient valence excited state XAS calculation has 5 more iodine 4d orbitals compared with the one in the FSSH calculation. 4 singlet and 4 triplet valence excited states were calculated to be consistent with FSSH calculation. The iodine 4 d orbital manifold is found about 50 eV lower than the 4 valence orbitals used in FSSH calculation, and their inclusion in the active space will barely influence the valence excited states. To simplify the calculation, we consider a particular PES to have the same index in both calculations (i.e., energy ordering is preserved). For future calculation for systems with close spaced PESs, FSSH calculation could be performed using the same active space as that of the excited XAS calculation to make sure that the valence excited states are consistent between both calculations; however, computational cost will increase significantly. The oscillator strengths between all 28 states are calculated in the RASSI module with spin-orbit coupling. Only the oscillator strengths that are related to the active, valence-excited PES were used for the probe absorption spectrum calculation. The core excitations were shifted in an *ad hoc* manner by −0.6 eV to compare with experimental data—this difference with respect to the ground state shift of −1.0 eV can be seen as compounding systematic errors in accuracy of both core and valence excitations and will be explored in future work. A smaller (than the ground state calculation above) Gaussian convolution (0.05 eV) was applied, in order not to inadvertently hide spectral features while averaging over multiple trajectories. By contrast, the larger ground state convolution (0.27 eV) used above serves as an approximation to the intrinsic ground state vibrational dynamics while computing the spectrum of a single, frozen molecular structure. Admittedly, previous work has also shown the importance of molecular dynamics sampling in the inner-shell absorption spectra of small molecules,[49] but that is not the focus of this study.

Since the main peaks of time-dependent XUV absorption located below 49 eV are mostly related to probing the singly occupied molecular orbitals (SOMOs) (which were originally doubly degenerate HOMO before the pump excited the valence orbitals), our on-the-fly XUV absorption spectrum should be reliable although the current setup is unable to handle higher-energy Rydberg states with sufficient accuracy.

Potential energy surface

Photodissociation of methyl iodide extends the C–I bond to form a methyl radical $CH_3^\bullet$ and a neutral I ($^2P_{3/2}$) or I* ($^2P_{1/2}$) atom. Note that the $5p^5$ electron configuration of the I atom couples total orbital angular momentum $L = 1$ (P) with the total spin $S = 1/2$, resulting in possible total angular momenta $J = 1 \pm \frac{1}{2}$, with Hund's rules, indicating that for greater than half filling, the higher $J = 3/2$ is the ground state and $J = 1/2$ is a spin-orbit excited state. Potential energy curves were calculated for the bond breaking process. During the C–I bond breaking process, as shown in the supplementary material movie1, C–I bond will extend after the photon excitation. Since the iodine atom is much heavier than the CH_3 fragment, the CH_3 fragment will move rapidly backward, while iodine atom moves slowly in the opposite direction. During the C–I bond extending process, the vibrational umbrella mode will be activated in the CH_3 fragment due to the inertia of the hydrogen atoms. For the PES calculation, the CH_3 fragment was fixed to be the ground state atomic structure of CH_3I, and the C–I bond is elongated from 1.88 to 4 Å along the original C–I bond direction. The $^3Q_0$ and $^1Q_1$ PESs cross when the C–I distance is 2.33 Å.

There are two major spin-orbit splittings in CH_3I, which are relevant to the transient XUV spectra we are simulating: one is the atomic splitting of iodine inner-shell 4d orbitals, accessible with the XUV probe, and the second one is the splitting of iodine valence

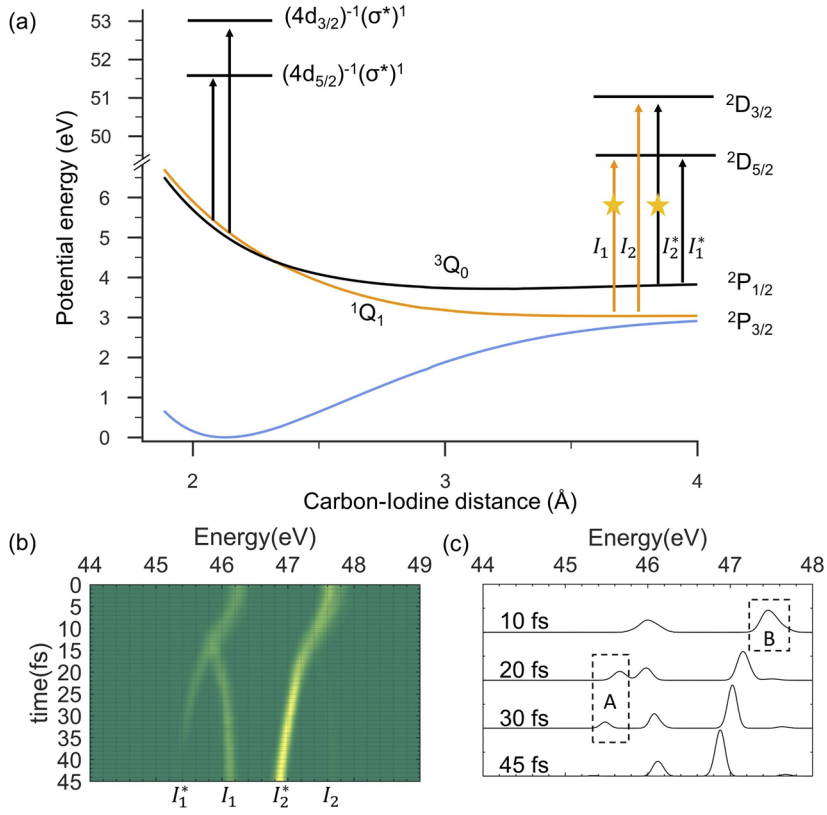

FIG. 4. (a) Potential energy curves for $CH_3I \rightarrow CH_3 + I$ with schematic inner-shell excitations from the I 4d orbital manifold. The photodissociation is modeled here by extending the C–I bond length from 1.88 to 4 Å, while keeping the geometry of the CH_3 fragment the same as it was in the molecular ground state of CH_3I. $^3Q_0$ and $^1Q_1$ PES cross when the C–I distance is 2.33 Å. The two excitations that correspond to the two major peaks at 45 fs in (b) are labeled with star symbols (☆). (b) Averaged XAS for 58 FSSH trajectories. (c) Snapshots of the averaged XAS at 10 fs, 20 fs, 30 fs, and 45 fs, respectively. Peaks in boxes A and B correspond to the transient A and transient B peaks in Ref. 3.

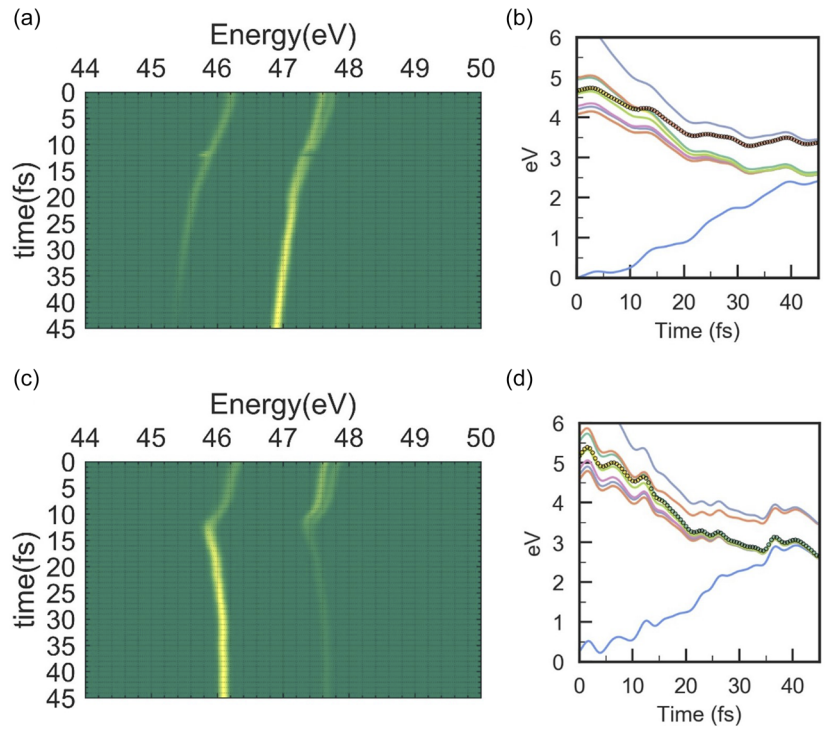

FIG. 5. XAS (a) and PES (b) of a trajectory that reaches the I* state. XAS (c) and PES (d) of a trajectory that reaches the I state. The active PES in (c) and (d) is labeled with black circles.

5p orbitals, accessible using the UV pump. In Fig. 4(b), there are two branched curves, whose energy separation is induced by the I 4d spin-orbit splitting—this is mostly a local atomic effect. There are two iodine atom states in the final product, I ($^2P_{3/2}$) or I* ($^2P_{1/2}$). In Fig. 4(a), the PESs converge to two branches: the orange and blue PESs converge to $^2P_{3/2}$ while the black PES converges to the $^2P_{1/2}$ state. For this reason, the FSSH trajectories only show two possible branches. Two representative trajectories are shown in Figs. 5(b) and 5(d). In both trajectories, the FSSH simulation started from the $^3Q_0$ state and reached the conical intersection around 12 fs. In our simulation of 58 trajectories, 71% of the trajectories stay on the $^3Q_0$ state, ending in the I* ($^2P_{1/2}$) state, while 29% of trajectories hop to the lower energy $^1Q_1$ state, ending in the I ($^2P_{3/2}$) state. The [I*]/([I] + [I*]) ratio is close to previous surface hopping simulation[16] and experiment[3,7,50,51] results, which ranges from 65% to 78%. The simulated XAS from both representative trajectories has distinct spectral characters, as shown in Figs. 5(a) and 5(c). In Fig. 5(a), the first peak (I^*_1) with lower energy shows small intensity and finally disappears at 40 fs. And the intensity of the second peak (I^*_2) gets stronger and stronger. In Fig. 5(c), the first 12 fs is similar to Fig. 5(b) because the trajectory starts and stays on the $^3Q_0$ state. After the conical intersection region, the trajectory hops to $^1Q_1$ state and the XAS peak makes a V turn and gradually converges to a value that is close to that at 0 fs. The first peak around 46 eV (I_1 peak) shows a stronger intensity, while the peak (I_2 peak) near 48 eV is weak but still visible until 45 fs. When the XAS of all the trajectories are superposed in Fig. 4(b), two branches of peaks appear, where the I^*_1 and I_1 contribute to the first branch and I^*_2 and I_2 comprise the second branch. The snapshots of the averaged XAS at 10 fs, 20 fs, 30 fs, and 45 fs are shown in Fig. 4(c). The origin of the transient A, B peaks in Ref. 3 can be understood clearly. The two major peaks are I_1 and I_2* peaks, and the height ratio represents the distribution of I ($^2P_{3/2}$) and I* ($^2P_{1/2}$) atoms in the final product. Transient A and transient B peaks are highlighted with boxes A and B, respectively, in Fig. 4(c). The transient A peak corresponds to the I_1* peak, and the transient B peak mainly results from the first 12 fs of the I_2* peak. Since the I_1* peak appears after the conical intersection, the transient A peak appears later than the transient B peak, which is consistent with Ref. 3.

CONCLUSION

In summary, a complete multireference pump-probe simulation method combining multireference excited state trajectories and associated transient XUV/X-ray absorption spectra was established and applied to study the UV-induced photodissociation of methyl iodide. Employing CASPT2 and RASSI implementations within OpenMolcas, and excited state trajectories via surface hopping implemented within SHARC, we can simulate the ultrafast evolution of the XAS. By choosing the core-orbital manifold within a restricted active space, limited to single-hole excitations, we can effectively simulate the XUV/X-ray probe of valence-excited states already treated within the complete active space formalism. This approach has great potential for interpreting or predicting measurements of the photo-induced dynamics of small molecules and is especially suitable for bond breaking or photodissociative processes.

SUPPLEMENTARY MATERIAL

See supplementary material for movie1: A FSSH trajectory of the C–I bond breaking process. Carbon, hydrogen, and iodine atoms are represented with cyan, white, and orange spheres, respectively. The C–I and H–I bond lengths in angstroms are labeled.

ACKNOWLEDGMENTS

Theoretical and computational work was performed by H.W. and D.P., within the Gas Phase Chemical Physics Program through the Chemical Sciences Division of Lawrence Berkeley National Laboratory (LBNL), supported by the U.S. Department of Energy (DOE), Office of Science, Office of Basic Energy Sciences, under Contract No. DE-AC02-05CH11231. M.O. acknowledges support from the Swedish Research Council (Contract No. VR 2015–03956). The authors acknowledge Sebastian Mai from the SHARC support team for his generous help with using the SHARC code. This work was supported by a user project at the Molecular Foundry (LBNL) under the same contract, with supercomputer time provided by the National Energy Research Scientific Computing Center (NERSC), and the Molecular Foundry and Lawrencium compute clusters, administered by the High-Performance Computing Services Group at LBNL.

REFERENCES

[1] A. Bhattacherjee and S. R. Leone, "Ultrafast x-ray transient absorption spectroscopy of gas-phase photochemical reactions: A new universal probe of photoinduced molecular dynamics," Acc. Chem. Res. **51**, 3203–3211 (2018).
[2] A. R. Attar *et al.*, "Femtosecond x-ray spectroscopy of an electrocyclic ring-opening reaction," Science **356**, 54–59 (2017).
[3] A. R. Attar, A. Bhattacherjee, and S. R. Leone, "Direct observation of the transition-state region in the photodissociation of CH_3I by femtosecond extreme ultraviolet transient absorption spectroscopy," J. Phys. Chem. Lett. **6**(24), 5072–5077 (2015).
[4] A. Bhattacherjee, C. D. Pemmaraju, K. Schnorr, A. R. Attar, and S. R. Leone, "Ultrafast intersystem crossing in acetylacetone via femtosecond x-ray transient absorption at the carbon K-edge," J. Am. Chem. Soc. **139**, 16576–16583 (2017).
[5] K. Schnorr *et al.*, "Tracing the 267 nm-induced radical formation in dimethyl disulfide using time-resolved x-ray absorption spectroscopy," J. Phys. Chem. Lett. **10**, 1382–1387 (2019).
[6] A. Bhattacherjee *et al.*, "Photoinduced heterocyclic ring opening of furfural: Distinct open-chain product identification by ultrafast x-ray transient absorption spectroscopy," J. Am. Chem. Soc. **140**, 12538–12544 (2018).
[7] S. J. Riley and K. R. Wilson, "Excited fragments from excited molecules: Energy partitioning in the photodissociation of alkyl iodides," Faraday Discuss. Chem. Soc. **53**, 132–146 (1972).
[8] S. Rosenwaks, "Photodissociation of vibrationally excited CH_3I," in *Vibrationally Mediated Photodissociation* (Royal Society of Chemistry, 2009), Vol. 159.
[9] R. Ogorzalek Loo, H.-P. Haerri, G. E. Hall, and P. L. Houston, "Methyl rotation, vibration, and alignment from a multiphoton ionization study of the 266 nm photodissociation of methyl iodide," J. Chem. Phys. **90**, 4222–4236 (1989).
[10] A. García-Vela, R. de Nalda, J. Durá, J. González-Vázquez, and L. Bañares, "A 4D wave packet study of the CH_3I photodissociation in the A-band. Comparison with femtosecond velocity map imaging experiments," J. Chem. Phys. **135**, 154306 (2011).
[11] R. de Nalda, J. G. Izquierdo, J. Durá, and L. Bañares, "Femtosecond multichannel photodissociation dynamics of CH_3I from the A band by velocity map imaging," J. Chem. Phys. **126**, 021101 (2007).

[12] M. E. Corrales *et al.*, "Structural dynamics effects on the ultrafast chemical bond cleavage of a photodissociation reaction," Phys. Chem. Chem. Phys. **16**, 8812–8818 (2014).
[13] R. de Nalda *et al.*, "A detailed experimental and theoretical study of the femtosecond A-band photodissociation of CH_3I," J. Chem. Phys. **128**, 244309 (2008).
[14] A. T. J. B. Eppink and D. H. Parker, "Methyl iodide A-band decomposition study by photofragment velocity imaging," J. Chem. Phys. **109**, 4758–4767 (1998).
[15] S. Yabushita and K. Morokuma, "Potential energy surfaces for rotational excitation of CH_3 product in photodissociation of CH_3I," Chem. Phys. Lett. **153**, 517–521 (1988).
[16] M. Kamiya and T. Taketsugu, "*Ab initio* surface hopping excited-state molecular dynamics approach on the basis of spin–orbit coupled states: An application to the A-band photodissociation of CH_3I," J. Comput. Chem. **40**, 456–463 (2019).
[17] A. T. J. B. Eppink and D. H. Parker, "Energy partitioning following photodissociation of methyl iodide in the A band: A velocity mapping study," J. Chem. Phys. **110**, 832–844 (1999).
[18] M. L. Murillo-Sánchez *et al.*, "Halogen-atom effect on the ultrafast photodissociation dynamics of the dihalomethanes CH_2ICl and CH_2BrI," Phys. Chem. Chem. Phys. **20**, 20766–20778 (2018).
[19] R. S. Mulliken, "Intensities in molecular electronic spectra X. Calculations on mixed-halogen, hydrogen halide, alkyl halide, and hydroxyl spectra," J. Chem. Phys. **8**, 382–395 (1940).
[20] L. Rui *et al.*, "Electronic curves crossing in methyl iodide by spin–orbit *ab initio* calculation," Chin. Phys. Lett. **25**, 1644–1645 (2008).
[21] H. F. King, R. E. Stanton, H. Kim, R. E. Wyatt, and R. G. Parr, "Corresponding orbitals and the nonorthogonality problem in molecular quantum mechanics," J. Chem. Phys. **47**, 1936–1941 (1967).
[22] P. G. Lykos and H. N. Schmeising, "Maximum overlap atomic and molecular orbitals," J. Chem. Phys. **35**, 288–293 (1961).
[23] A. T. B. Gilbert, N. A. Besley, and P. M. W. Gill, "Self-consistent field calculations of excited states using the maximum overlap method (MOM)," J. Phys. Chem. A **112**, 13164–13171 (2008).
[24] K. Lopata, B. E. Van Kuiken, M. Khalil, and N. Govind, "Linear-response and real-time time-dependent density functional theory studies of core-level near-edge x-ray absorption," J. Chem. Theory Comput. **8**, 3284–3292 (2012).
[25] Y. Shao, M. Head-Gordon, and A. I. Krylov, "The spin–flip approach within time-dependent density functional theory: Theory and applications to diradicals," J. Chem. Phys. **118**, 4807–4818 (2003).
[26] V. Veryazov, P. Å. Malmqvist, and B. O. Roos, "How to select active space for multiconfigurational quantum chemistry?," Int. J. Quantum Chem. **111**, 3329–3338 (2011).
[27] K. Andersson and B. O. Roos, "Multiconfigurational second-order perturbation theory," in *Modern Electronic Structure Theory* (World Scientific Publishing Company, 1995), pp. 55–109.
[28] V. Sauri *et al.*, "Multiconfigurational second-order perturbation theory restricted active space (RASPT2) method for electronic excited states: A benchmark study," J. Chem. Theory Comput. **7**, 153–168 (2011).
[29] M. Richter, P. Marquetand, J. González-Vázquez, I. Sola, and L. González, "SHARC: *Ab initio* molecular dynamics with surface hopping in the adiabatic representation including arbitrary couplings," J. Chem. Theory Comput. **7**, 1253–1258 (2011).
[30] S. Mai, P. Marquetand, and L. González, "Nonadiabatic dynamics: The SHARC approach," Wiley Interdiscip. Rev.: Comput. Mol. Sci. **8**, e1370 (2018).
[31] S. Mai, M. Richter, M. Heindl, M. F. S. J. Menger, A. Atkins, M. Ruckenbauer, F. Plasser, M. Oppel, P. Marquetand, and L. González, SHARC2.0: Surface Hopping Including Arbitrary Couplings – Program Package for Non-Adiabatic Dynamics, 2018, available at https://sharc-md.org.
[32] S. Mai, M. Richter, P. Marquetand, and L. González, "The DNA nucleobase thymine in motion – Intersystem crossing simulated with surface hopping," Chem. Phys. **482**, 9–15 (2017).
[33] J. P. Zobel, J. J. Nogueira, and L. González, "Mechanism of ultrafast intersystem crossing in 2-nitronaphthalene," Chem. - A Eur. J. **24**, 5379–5387 (2018).
[34] T. Schnappinger *et al.*, "*Ab initio* molecular dynamics of thiophene: The interplay of internal conversion and intersystem crossing," Phys. Chem. Chem. Phys. **19**, 25662–25670 (2017).
[35] R. J. Squibb *et al.*, "Acetylacetone photodynamics at a seeded free-electron laser," Nat. Commun. **9**, 63 (2018).
[36] I. Josefsson *et al.*, "*Ab initio* calculations of x-ray spectra: Atomic multiplet and molecular orbital effects in a multiconfigurational SCF approach to the L-edge spectra of transition metal complexes," J. Phys. Chem. Lett. **3**, 3565–3570 (2012).
[37] M. Lundberg and M. G. Delcey, "Multiconfigurational approach to x-ray spectroscopy of transition metal complexes BT," in *Transition Metals in Coordination Environments: Computational Chemistry and Catalysis Viewpoints*, edited by E. Broclawik, T. Borowski, and M. Radoń (Springer International Publishing, 2019), pp. 185–217.
[38] P. Å. Malmqvist, B. O. Roos, and B. Schimmelpfennig, "The restricted active space (RAS) state interaction approach with spin–orbit coupling," Chem. Phys. Lett. **357**, 230–240 (2002).
[39] J. Finley, P.-Å. Malmqvist, B. O. Roos, and L. Serrano-Andrés, "The multi-state CASPT2 method," Chem. Phys. Lett. **288**, 299–306 (1998).
[40] B. A. Hess, "Relativistic electronic-structure calculations employing a two-component no-pair formalism with external-field projection operators," Phys. Rev. A **33**, 3742–3748 (1986).
[41] M. Douglas and N. M. Kroll, "Quantum electrodynamical corrections to the fine structure of helium," Ann. Phys. **82**, 89–155 (1974).
[42] B. O. Roos, R. Lindh, P. A. Malmqvist, V. Veryazov, and P. O. Widmark, "Main group atoms and dimers studied with a new relativistic ANO basis set," J. Phys. Chem. A **108**, 2851–2858 (2004).
[43] B. O. Roos, R. Lindh, P.-Å. Malmqvist, V. Veryazov, and P.-O. Widmark, "New relativistic ANO basis sets for transition metal atoms," J. Phys. Chem. A **109**, 6575–6579 (2005).
[44] B. A. Heß, C. M. Marian, U. Wahlgren, and O. Gropen, "A mean-field spin-orbit method applicable to correlated wavefunctions," Chem. Phys. Lett. **251**, 365–371 (1996).
[45] M. Guo, L. K. Sørensen, M. G. Delcey, R. V. Pinjari, and M. Lundberg, "Simulations of iron K pre-edge X-ray absorption spectra using the restricted active space method," Phys. Chem. Chem. Phys. **18**, 3250–3259 (2016).
[46] J. C. Tully, "Molecular dynamics with electronic transitions," J. Chem. Phys. **93**, 1061–1071 (1990).
[47] M. Ben-Nun, J. Quenneville, and T. J. Martínez, "*Ab initio* multiple spawning: Photochemistry from first principles quantum molecular dynamics," J. Phys. Chem. A **104**, 5161–5175 (2000).
[48] G. Granucci, M. Persico, and A. Zoccante, "Including quantum decoherence in surface hopping," J. Chem. Phys. **133**, 134111 (2010).
[49] J. S. Uejio, C. P. Schwartz, R. J. Saykally, and D. Prendergast, "Effects of vibrational motion on core-level spectra of prototype organic molecules," Chem. Phys. Lett. **467**, 195–199 (2008).
[50] W. P. Hess, S. J. Kohler, H. K. Haugen, and S. R. Leone, "Application of an InGaAsP diode laser to probe photodissociation dynamics: I^* quantum yields from *n*- and *i*-C_3F_7I and CH_3I by laser gain vs absorption spectroscopy," J. Chem. Phys. **84**, 2143–2149 (1986).
[51] A. V. Baklanov, M. Aldener, B. Lindgren, and U. Sassenberg, "R2PI detection of the quantum yields of $I(^2P_{1/2})$ and $I(^2P_{3/2})$ in the photodissociation of C_2F_5I, *n*-C_3F_7I, *i*-C_3F_7I and CH_3I," Chem. Phys. Lett. **325**, 399–404 (2000).